LA-UR- 04-7076

Approved for public release;
distribution is unlimited.

Title:	SVD Analysis for Radiographic Object Reconstruction III: Total Variation Regularization
Author(s):	Thomas J. Asaki (CCS-2) Kevin R. Vixie (T-7)
Submitted to:	LANL Report

Los Alamos
NATIONAL LABORATORY

Form 836 (8/00)

SVD Analysis for Radiographic Object Reconstruction III: Total Variation Regularization

Thomas J. Asaki and Kevin R. Vixie

August 2004

Abstract

This report presents total variation (TV) regularization applied to tomographic reconstruction of the BCO4 (British calibration object #4). We outline some basic concepts of TV and modifications necessary for successful tomography. Our basic approach considers a 3D reconstruction to be a compilation of independent 2D slices. Each method is applied to proton radiography areal density data supplied by P-25 from experiments completed at LANSCE. Reconstructions are not yet quantitatively analyzed because of the lack of object metrology. Nevertheless, TV regularized reconstructions are shown to be superior to the filtered backprojection solution and prior-regularized SVD based solutions in terms of local density determination and density discontinuity preservation. In addition the TV solution naturally suppresses reconstruction noise and multiple-view placement artifacts. Ongoing and future improvements are discussed.

1. Introduction

For decades, tomography methods have enjoyed great successes in medical imaging. Accurate interior density and material maps of the human body can be obtained in a matter of an hour. These successes, however, rely heavily on the availability of hundreds of transmission radiographs at different viewing angles. Advanced radiography facilities at LANL, both present and future, however, have at most several views. The sparsity of available data is responsible for a large ambiguity in a reconstructed object (the projection operator has a large null space). The central problem in sparse-data tomography is to reduce this ambiguity through principled regularization.

Previous work proposed the use of a prior-knowledge based approach that utilized a singular value decomposition (SVD) description of the projection matrix. For certain types of objects and often minimal prior knowledge the results were quite good.

We begin with a discussion of LANSCE proton radiographic data and the test object used in this study. Then we describe TV outlining a simple approach for use with radiographic data. Next, a results section presents the various reconstructions and comparisons with the test object. Concluding remarks discuss the merits of the reconstructions and point to possible future improvements.

2. Test Object and Proton Radiograph Data

The test object for this study is the British calibration object designated BCO4. A schematic drawing is shown in Fig. 1. It consists of an aluminum ($\rho = 2.71$ g/cm^3) body and a central insert is made of lead ($\rho = 19.3$ g/cm^3). The object is solid except for the two small cone shaped cavities within the lead insert. Solid lines delineate the material boundaries. This drawing was made from the best-available data provided to us and can be considered approximately to scale. The figure also shows three 2D slices (horizontal dashed lines) used for all example reconstructions. In addition, the vertical dashed line and lower case roman letters indicate locations of density lineouts also used to compare

reconstruction methods

The BCO4 was chosen because proton radiographs of this object exist for 30 separate views from experiments at Line C at LANSCE. The beam energy for the experiments was approximately 800 MeV. The raw data exists as particle counts or beam intensities at each detector pixel. We currently rely on P-25 to provide the conversion to areal density, which we then use in density reconstructions. We re-binned the data (using linear interpolation) from 1249 data values per line to 208 data values per line. The object reconstructions were performed on a 208 by 208 voxel grid for each slice. These dimension reductions are currently necessary for computational efficiency on a desktop computer. It is not a limitation of the method.

This report considers several 2D slices of the BCO4 data. A full 3D reconstruction can be composed of stacked 2D reconstructions or by considering the full 3D solution. At present the 3D construction is too computationally intensive for detailed studies. The reconstructions also ignore any problems associated with outscatter and chromatic limbing, as well as any scattering effects not accounted for in the data conversion from intensity to areal density.

3. Total Variation Regularization

Our choice for regularizing tomographic reconstructions is total variation (TV) because it favors the piecewise smooth solution that projects to the given noisy data to within some tolerance. TV regularizations preserve discontinuities in density if they are consistent with the data. One natural consequence of TV regularization is the suppression or elimination of small-scale features in the reconstruction. Such features include anything on the order of the size of a voxel, including noise and object texture. For radiography applications we utilize a generalized form of the standard TV formulation given by

$$\min_{x \in X} \left\{ F(x) \equiv \alpha \int |\nabla x| dA + \tfrac{1}{2} \|Px - d\|_2^2 \right\} \qquad (1)$$

where P is the linear projection operator connecting the object space X to the data space, x is a reconstruction, d is the noisy data, and α is a weighting parameter. The object x is a collection of densities on a square voxel grid of known size. The data d is a collection of projected masses on pixel arrays of known size and orientation. The projection operator P is taken to be the linear geometric projection assuming a plane parallel beam experiment. The parameter α can be estimated from some knowledge of the data noise characteristics. For example, if the noise is additive Gaussian with mean zero and standard deviation s we have $\alpha = s^2$. In general, for radiography applications the noise is expected to be Poisson with variance dependent upon intensity. For this analysis we assume that the noise is reasonably well described by a single variance s^2.

This regularization differs from a typical image denoising application in that the data fidelity constraint (last term in Eq. 1) is applied to a linear projection of the image rather than on the image itself. We utilize the Lagged Diffusivity Fixed Point minimization method given by Vogel [1] to solve Eq. 1. In this framework α serves as a Lagrange multiplier.

3. Reconstruction Methods

Five reconstruction methods were applied to each slice. We have described some cases previously [2], but we include brief descriptions of all for completeness.

Filtered Backprojection (FPB) The filtered backprojection solution is obtained using the publically available Matlab code of Adel Faridani [3]. A ramp filter was used and the result was mass corrected.

Noise-constrained singular value decomposition (SVD) The projection matrix is partially inverted using a truncated set of singular vectors corresponding to the singular value set $\sigma_i \le s\sigma_{\max}$. In this way we reconstruct object features without noise amplification. This noise-level constrained inversion is the best low-dimensional reconstruction in the absence of prior knowledge and regularization schemes and

reconstruction quality is relatively insensitive to the choice of realistic s [4].

Nonnegative prior SVD (pSVD) The nonnegativity solution is obtained through an iterative process $x_{new} = x_{old} + (I - P)y$ with prior $y = \max(0, x_{old})$. The iteration is terminated when $\|Px - d\|_2^2 \approx 2s^2$. This reconstruction has the advantage of nudging the solution toward a data-satisfying positive-density object. The solution is also desirable over the truncated SVD solution because it reduces $2v$-fold symmetry artifacts (from v independent views) and more accurately identifies sharp density discontinuities [5].

Total variation prior SVD (TV-SVD) A TV regularized solution (Eq. 1) of large α was used as a prior estimation within a pSVD iterative solution (described above). While this method does not guarantee good noise statistics in the final solution, the good quality of the prior leads to a good solution in practice.

Noise-constrained TV (TV) For this method, the parameter α is chosen so that once the minimization in Eq. 1 is complete we have $\|Px - d\|_2^2 \approx 2s^2 = 2\alpha$. In this way, not only do we obtain a solution with low variation but the projection of the solution differs from the noisy data by a variance that is known to be approximately correct. This procedure is recursive; the minimization must be performed several times for different values of α before the desired reconstruction is determined.

4. BCO4 Reconstructions and Analysis

Three 2D slices of the BCO4 were chosen for reconstruction. Figure 2 shows representative proton radiographs with dashed lines indicating the slice locations. Reconstructions of the three selected slices by the five methods and for 12, 18, 24, and 30 views are shown in Figs. 3 through 14.

4.1 General Observations

As expected, all slices are best reconstructed using more views. Visually, only slice-A is well reconstructed with only 12 views. Other slices continue to improve with added views even with 30 views. Slice-A is reconstructed well because it contains only a single material. The density of the inner material (Pb) is poorly recovered; this issue is discussed later. Methods that incorporate regularized inversions perform better in identifying material boundaries and regions of constant density. In addition, TV methods eliminate $2v$-fold artifacts. Finally, we note the 'shadows' cast by the dense central object in Fig. 10e. These reconstruction anomalies appear to be related to some systematic problem with the data (possibly a data centering issue?) since reconstructions of other objects do not show this effect.

4.2 Density Determination

For density determination two major assumptions are made. First, the areal-density data is assumed to be converted from intensity radiographs according to the best available calibration data for aluminum. This means that our reconstructions are density maps of aluminum (even if unphysical). Second, because we do not have the actual detector pixel size, we allow a single density scaling parameter. This essentially lets us choose the normal density of aluminum (2.71 g/cm^3) to correspond to the reconstruction intensity of the central portion of Fig. 6d. Thus, the mean aluminum density (everything not Pb) for each picture is bound to be quite close to the correct density, but variations will depend upon the particular reconstruction method. The density of the insert is reconstructed as if it were also made of aluminum.

Several density lineouts are shown in Figs. 15-17. The lineout locations are indicated by the points in Fig. 1 labeled by lower case roman letters. For example, Fig. 15 shows lineout c which is within slice C and along the path indicated by the vertical dashed line of Fig. 1. The various colors indicate reconstructions by the various methods: (cyan) FBP; (black) SVD; (blue) pSVD; (green) TV; and (red) TV-SVD. These lineouts show a definite left-to-right density increase indicating a weakness in the conversion process from radiograph intensity to areal density data. In spite of the apparent data problems, the TV-SVD reconstructions have several nice properties: excellent edge

detection; good noise reduction; and zero-density retention in regions of expected zero density. The pSVD solution has better zero-density retention because this feature is built in to the driving prior, but has poor quality (similar to FBP) in regions of nonzero density. Lead (Pb) densities are not recovered in this analysis, as discussed previously.

5. Conclusions and Future Work

Overall, TV-based regularized reconstructions preserve desirable object features such as density discontinuities while reducing noise and limited-number-of-view artifacts. We are prevented from further quantitative analysis by lack of quantitative metrology and experiment details. Also, we have not attempted a true multiple material reconstruction. We continue to explore gradient-based regularization methods that incorporate minimal prior knowledge. Notably, we are exploring adaptive methods for edge retention and density preserving data fidelity. These methods are currently implemented in Abel inversion tomography settings and are being explored as possible candidates for 3D object reconstruction.

6. References

[1] Curtis R. Vogel, "*Computational methods for inverse problems*," SIAM (2002).

[2] Thomas J. Asaki, Patrick R. Campbell, and Kevin R. Vixie, "*A Comparison of Tomographic Reconstruction Methods for 3D Objects Using a Limited Number of Noisy Radiographic Views*," LA-UR-03-6196 (2003).

[3] Adel Faridani, FBP sMatlab code available through: http://oregonstate.edu/~faridana/ (2001)

[4] Thomas J. Asaki and Kevin R. Vixie, "*SVD analysis for radiographic object reconstruciton I: Initial results*," LA-UR-01-6534 (2001).

[5] Thomas J. Asaki and Kevin R. Vixie, "*SVD analysis for radiographic object reconstruction II: Null space enhancements using minimal constraints*," LA-UR-03-5937 (2003).

[6] Brian A. Temple, "*Step wedge simulations for the AGS Experiment E955*," LANL Research Note, LA-UR-02-6891 (2002).

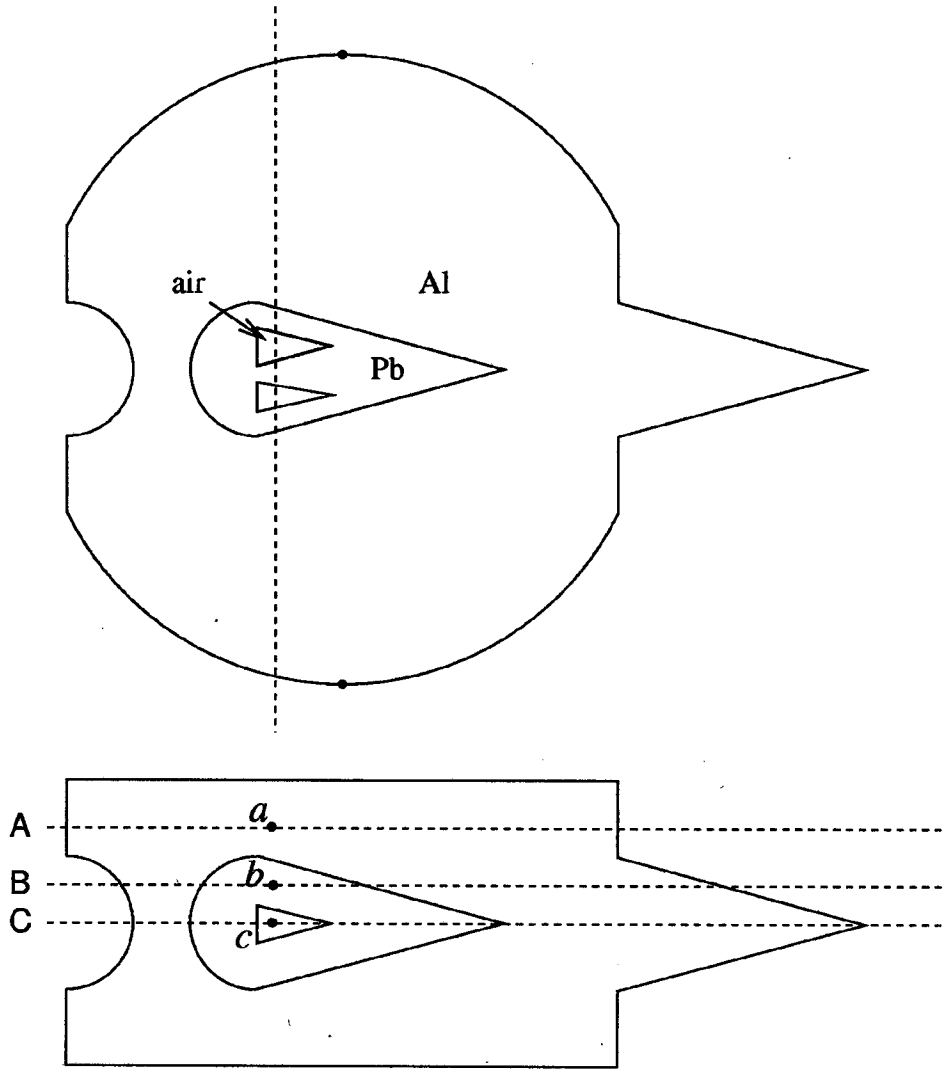

Figure 1. Schematic drawing of the BCO4. Solid lines delineate between different materials. The outer material is aluminum (Al) and the central insert is lead (Pb) with two machined voids. The top illustration is a horizontal plane slice through the BCO4 center; the bottom illustration is a vertical plane slice through the center. Three horizontal dashed lines, labeled by capital roman letters, indicate 2D slices used for example reconstructions. Lower case roman letters and the vertical dashed line indicate locations of density lineouts used to compare reconstruction methods.

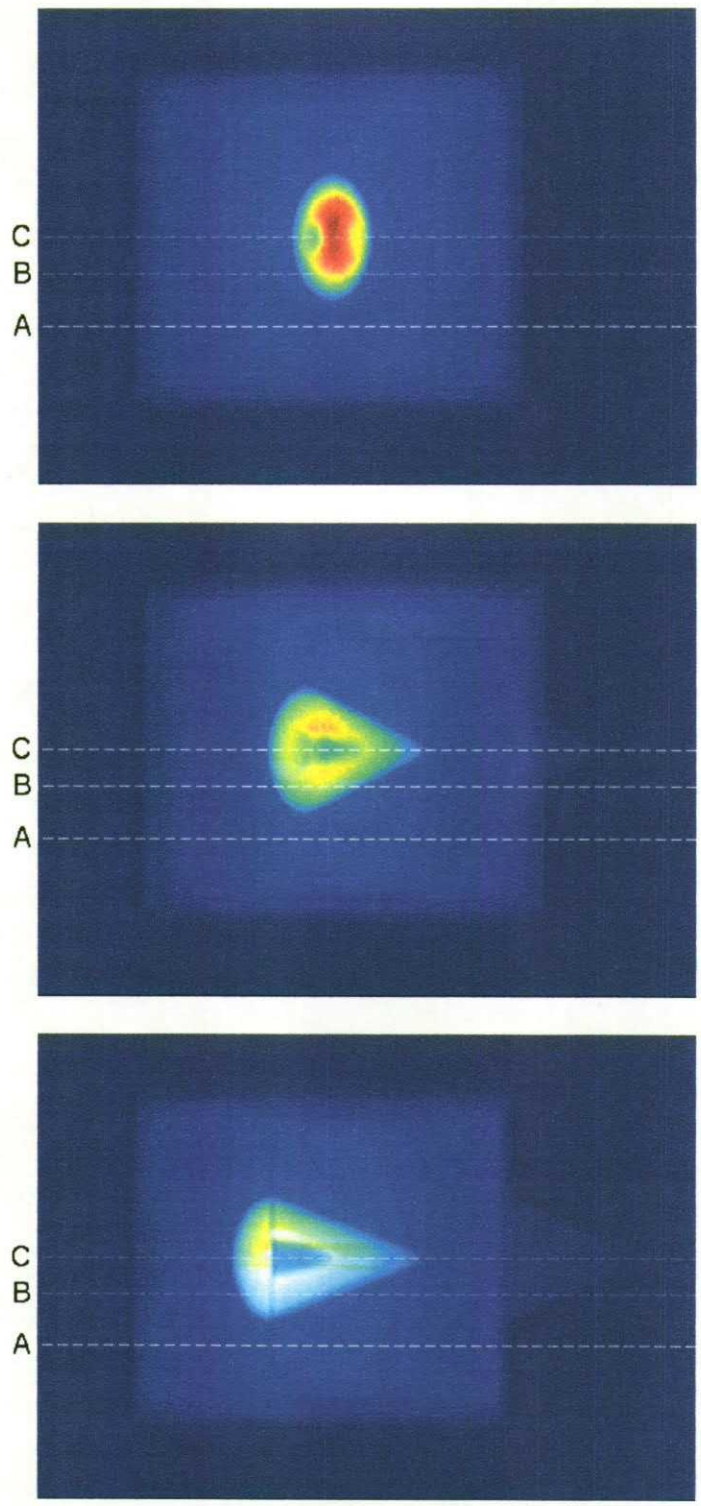

Figure 2. Three representative proton radiographs of the BCO4 are shown for orientation angles of 0, 48 and 90 degrees, respectively. The dashed lines (A, B, and C) indicate the horizontal slices used in the reconstruction algorithms.

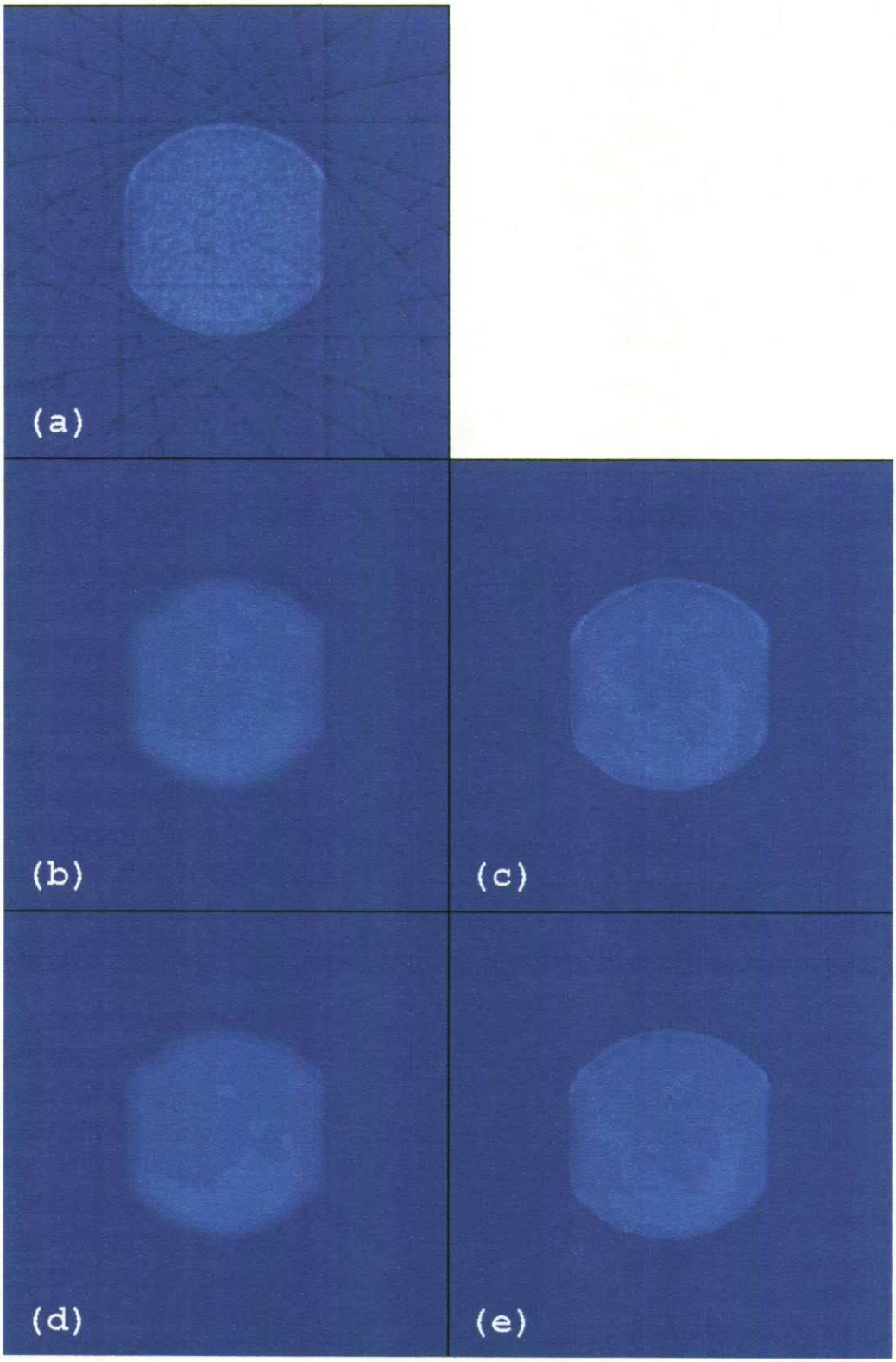

Figure 3. BCO4 slice-A 12-view reconstructions: (a) FBP; (b) SVD; (c) pSVD; (d) TV; and (e) TV-SVD.

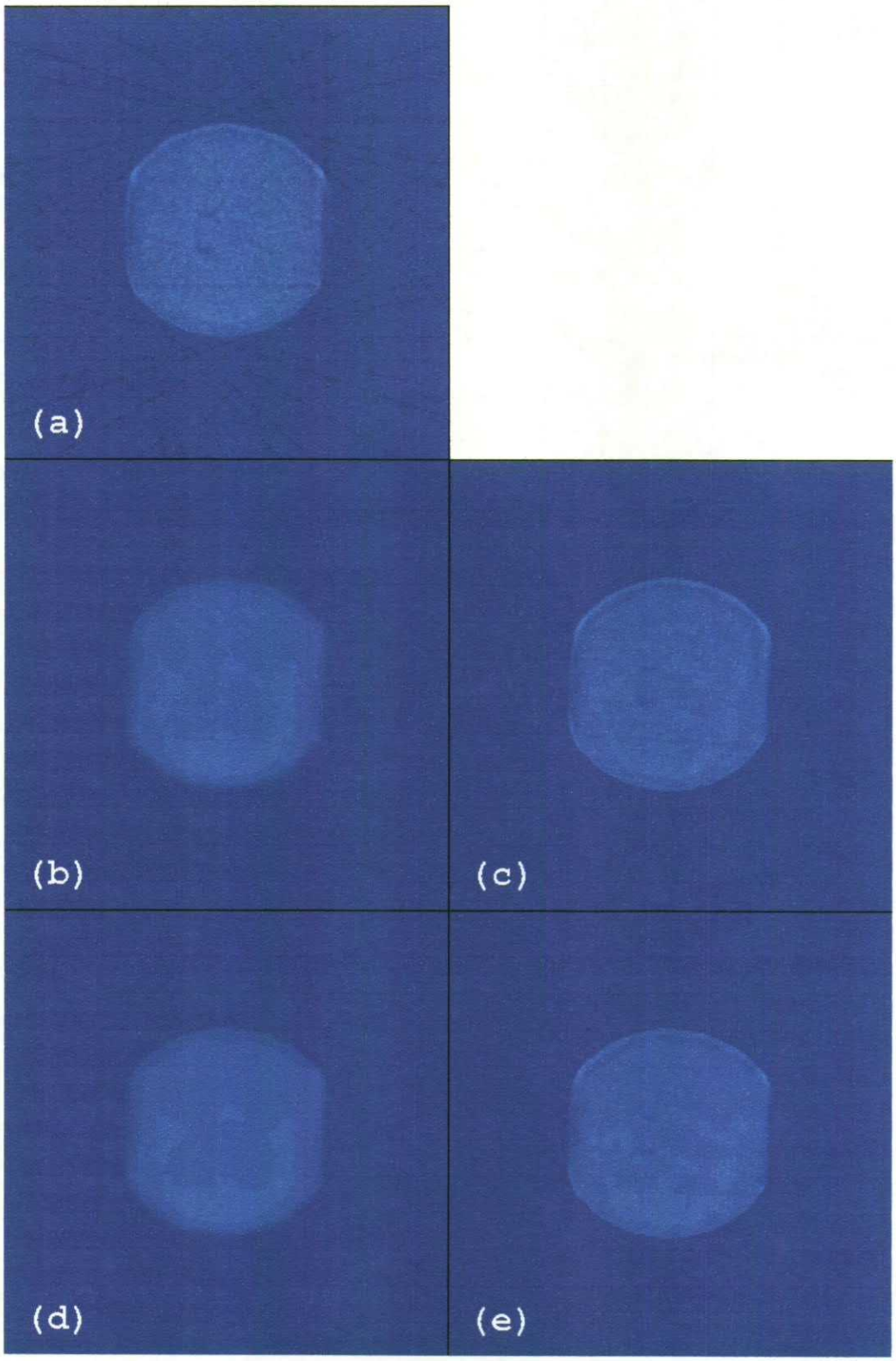

Figure 4. BCO4 slice-A 18-view reconstructions: (a) FBP; (b) SVD; (c) pSVD; (d) TV; and (e) TV-SVD.

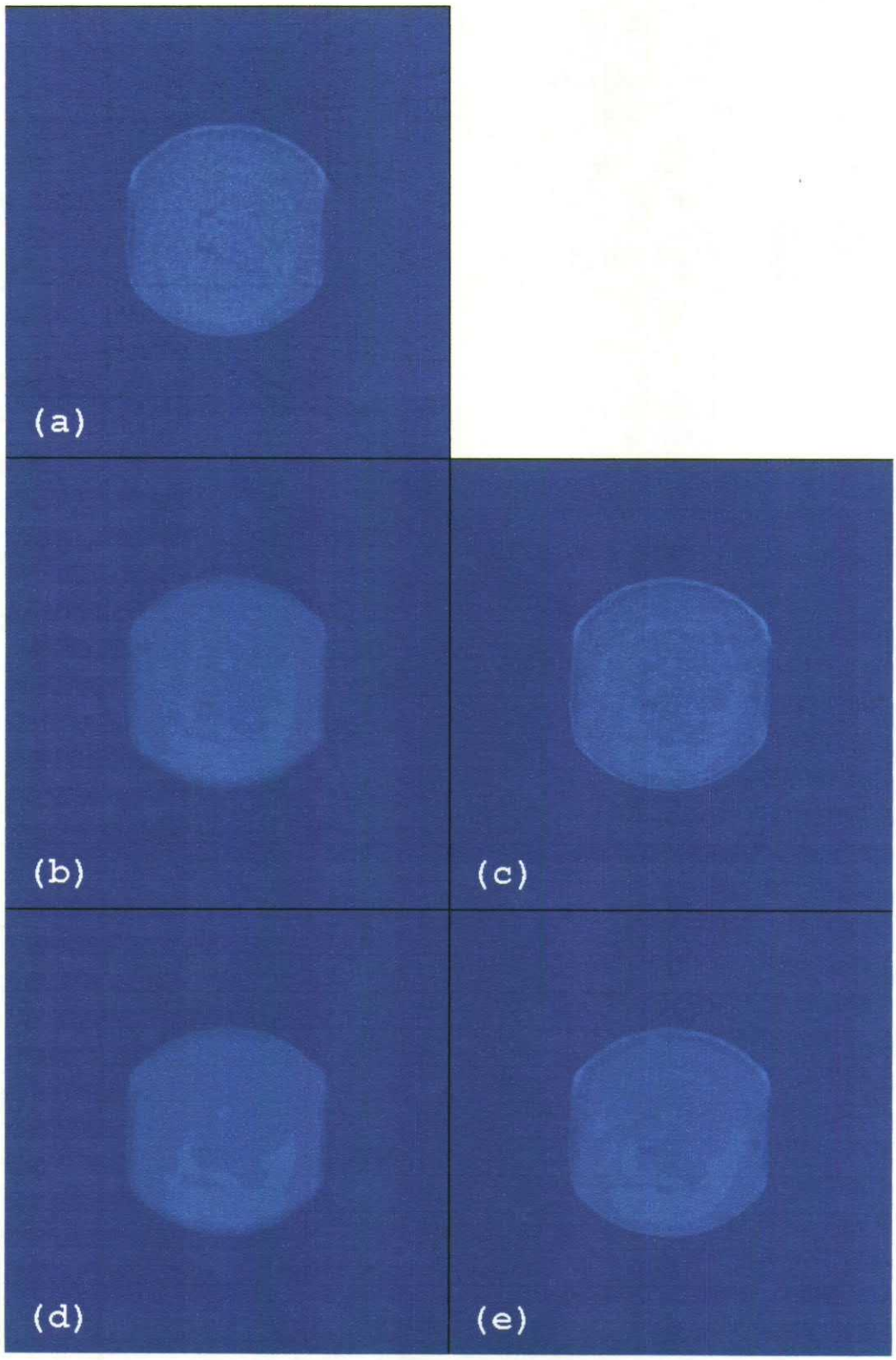

Figure 5. BCO4 slice-A 24-view reconstructions: (a) FBP; (b) SVD; (c) pSVD; (d) TV; and (e) TV-SVD.

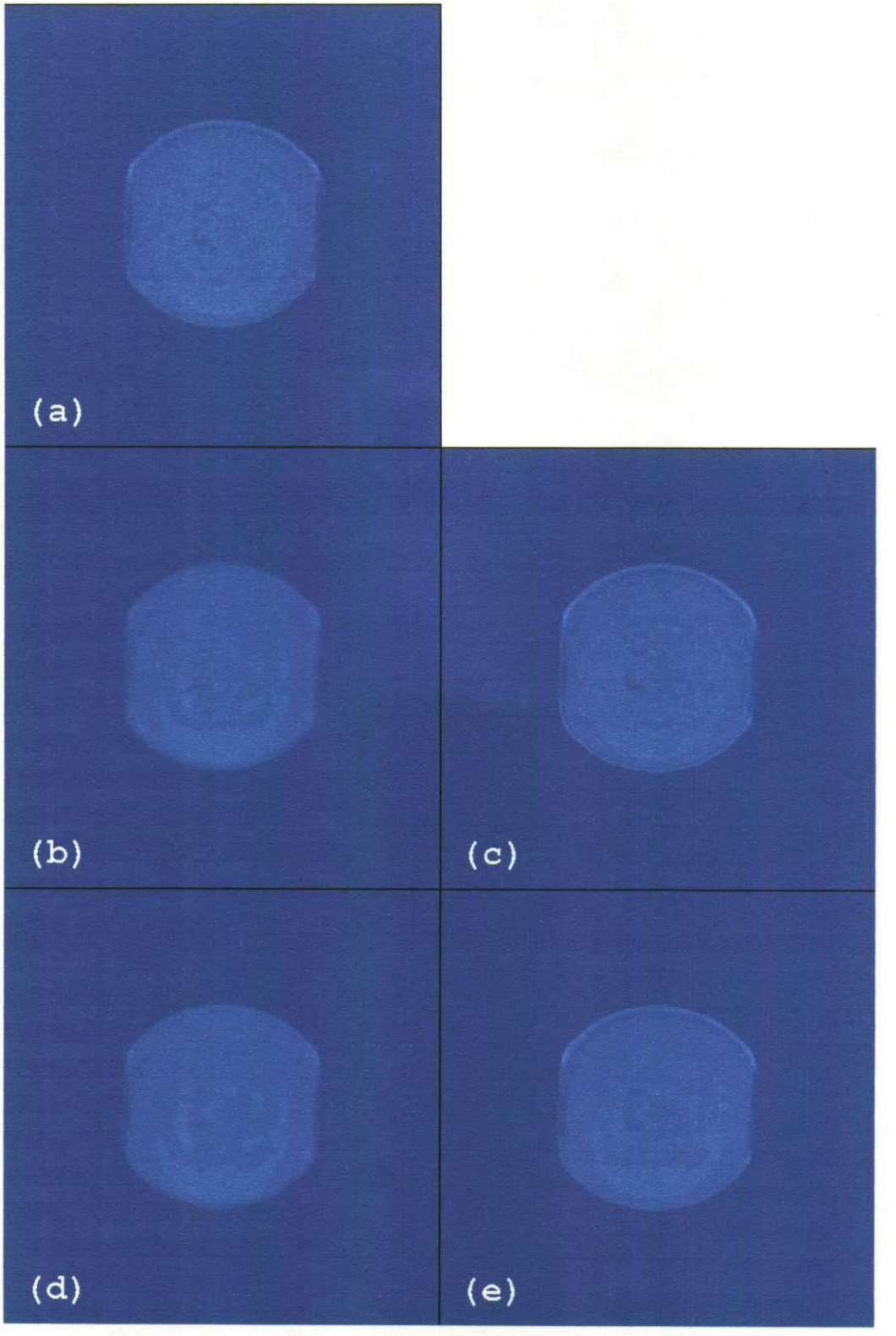

Figure 6. BCO4 slice-A 30-view reconstructions: (a) FBP; (b) SVD; (c) pSVD; (d) TV; and (e) TV-SVD.

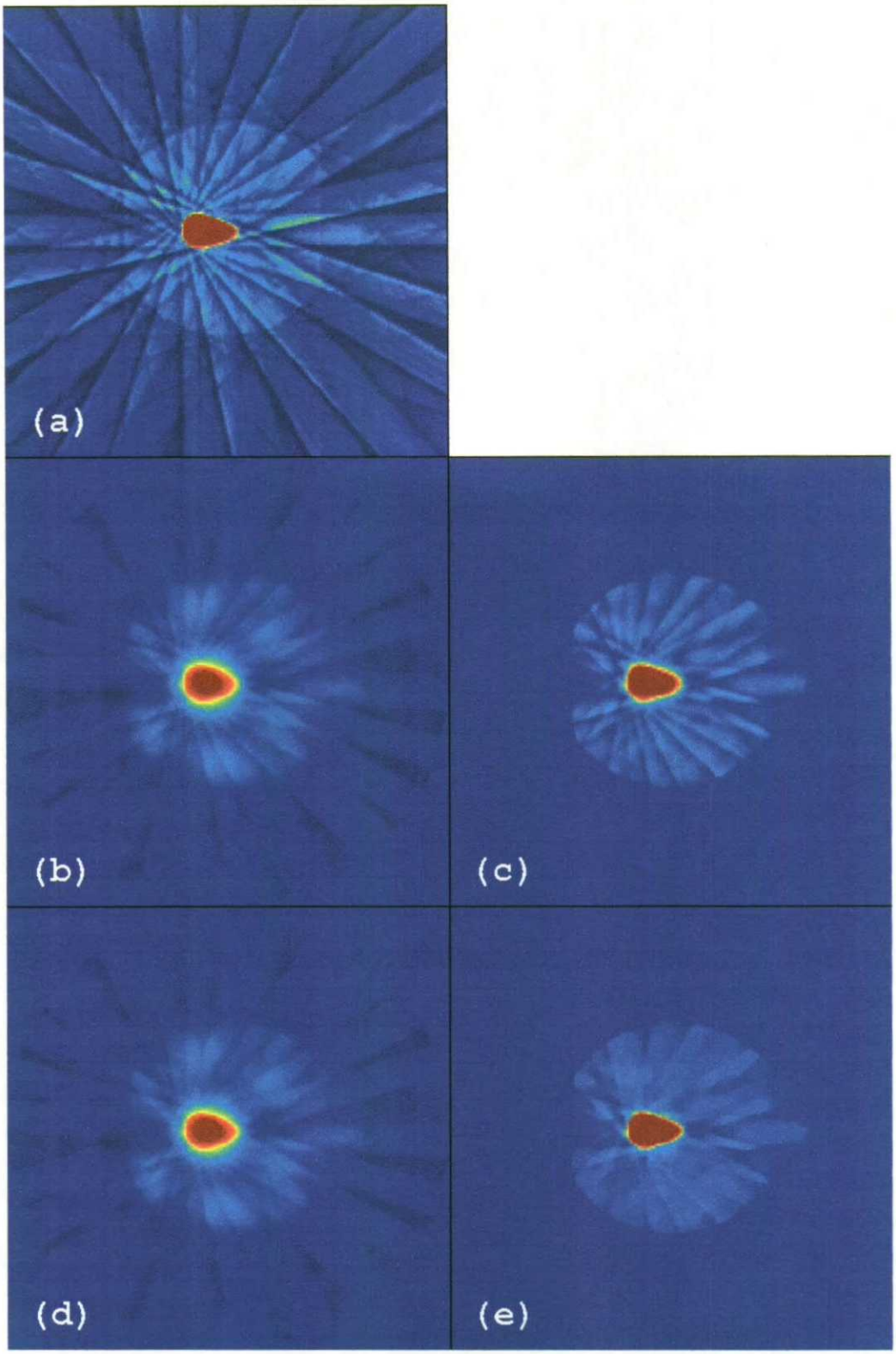

Figure 7. BCO4 slice-B 12-view reconstructions: (a) FBP; (b) SVD; (c) pSVD; (d) TV; and (e) TV-SVD.

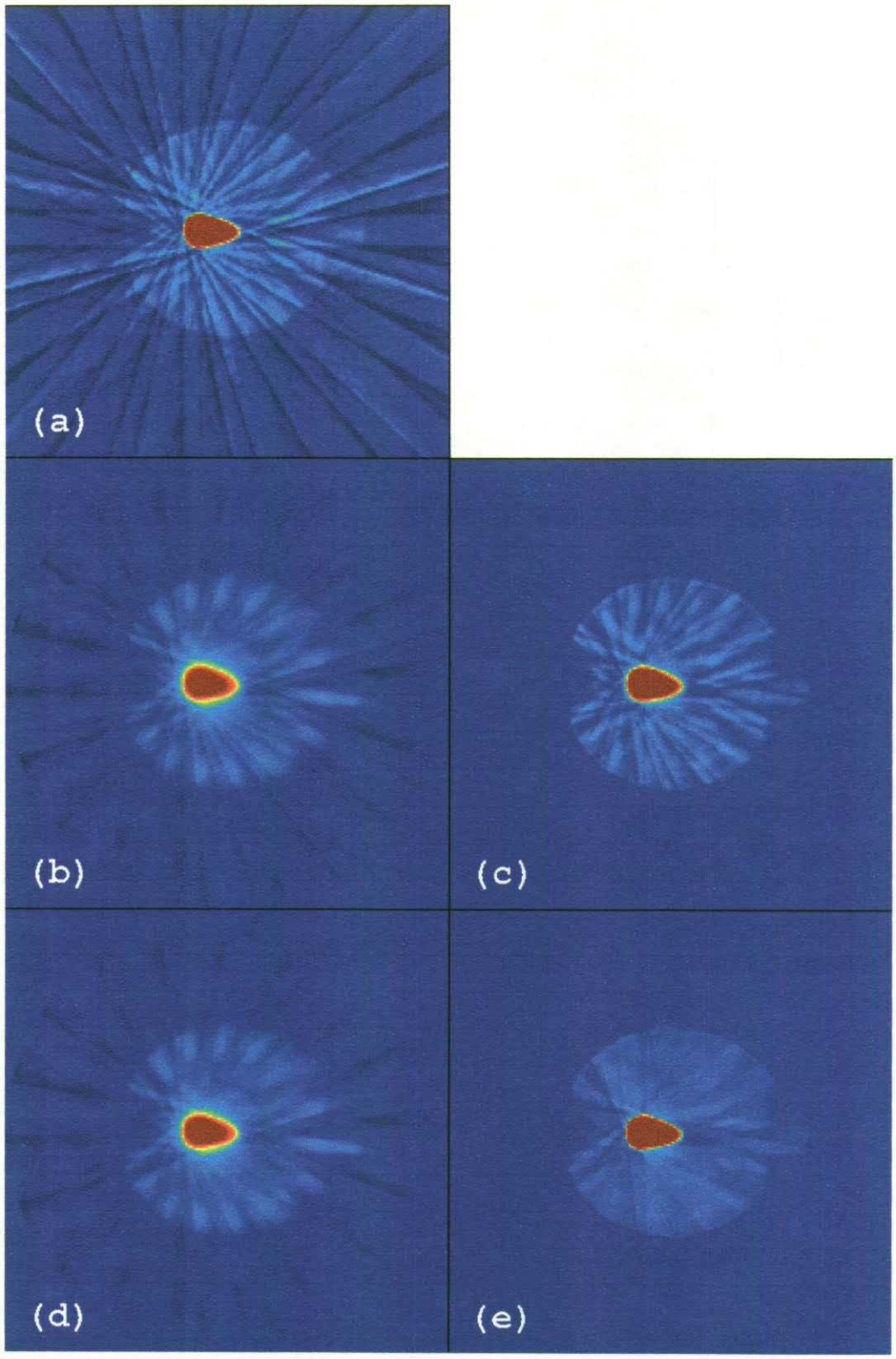

Figure 8. BCO4 slice-B 18-view reconstructions: (a) FBP; (b) SVD; (c) pSVD; (d) TV; and (e) TV-SVD.

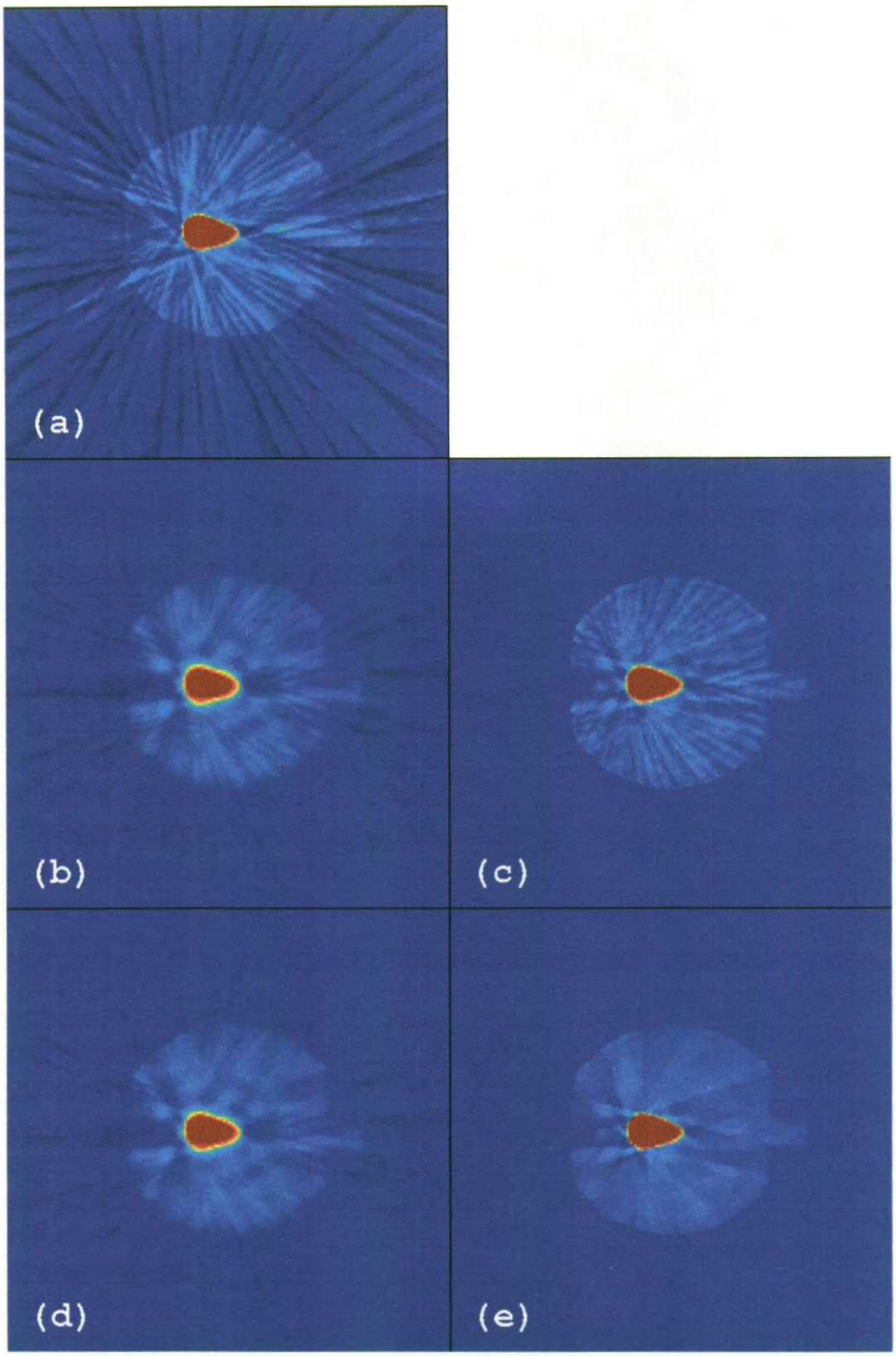

Figure 9. BCO4 slice-B 24-view reconstructions: (a) FBP; (b) SVD; (c) pSVD; (d) TV; and (e) TV-SVD.

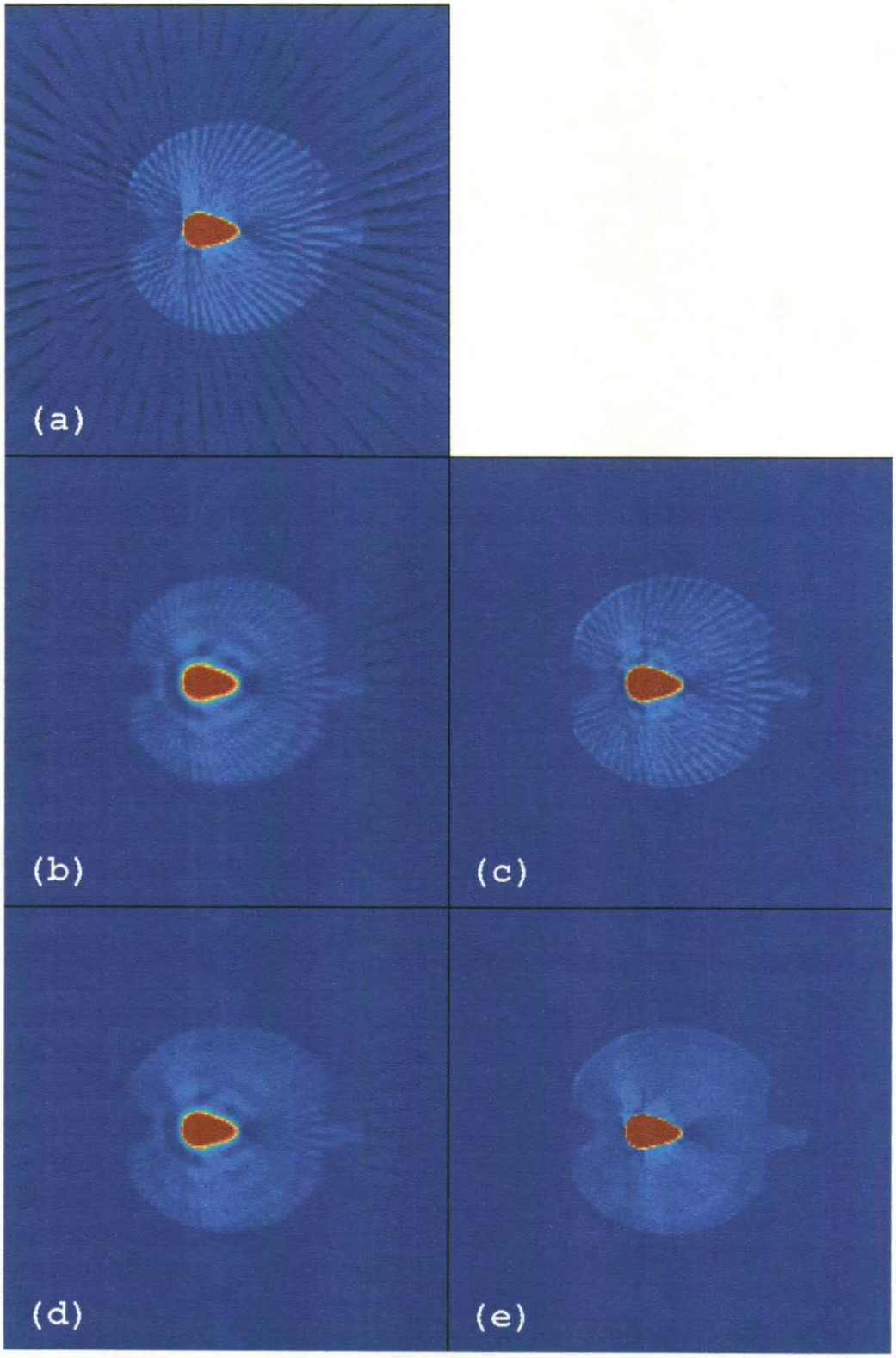

Figure 10. BCO4 slice-B 30-view reconstructions: (a) FBP; (b) SVD; (c) pSVD; (d) TV; and (e) TV-SVD.

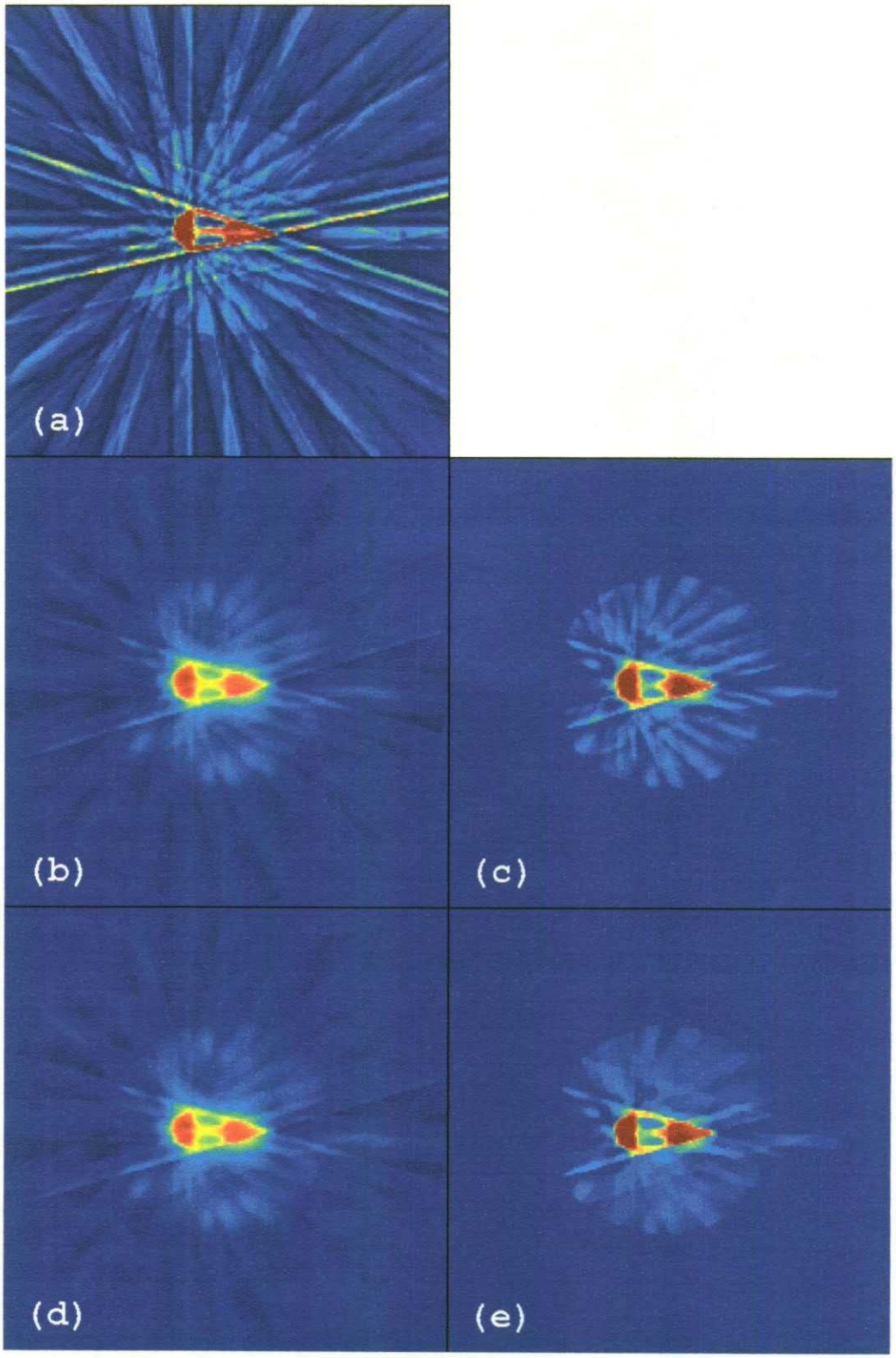

Figure 11. BCO4 slice-C 12-view reconstructions: (a) FBP; (b) SVD; (c) pSVD; (d) TV; and (e) TV-SVD.

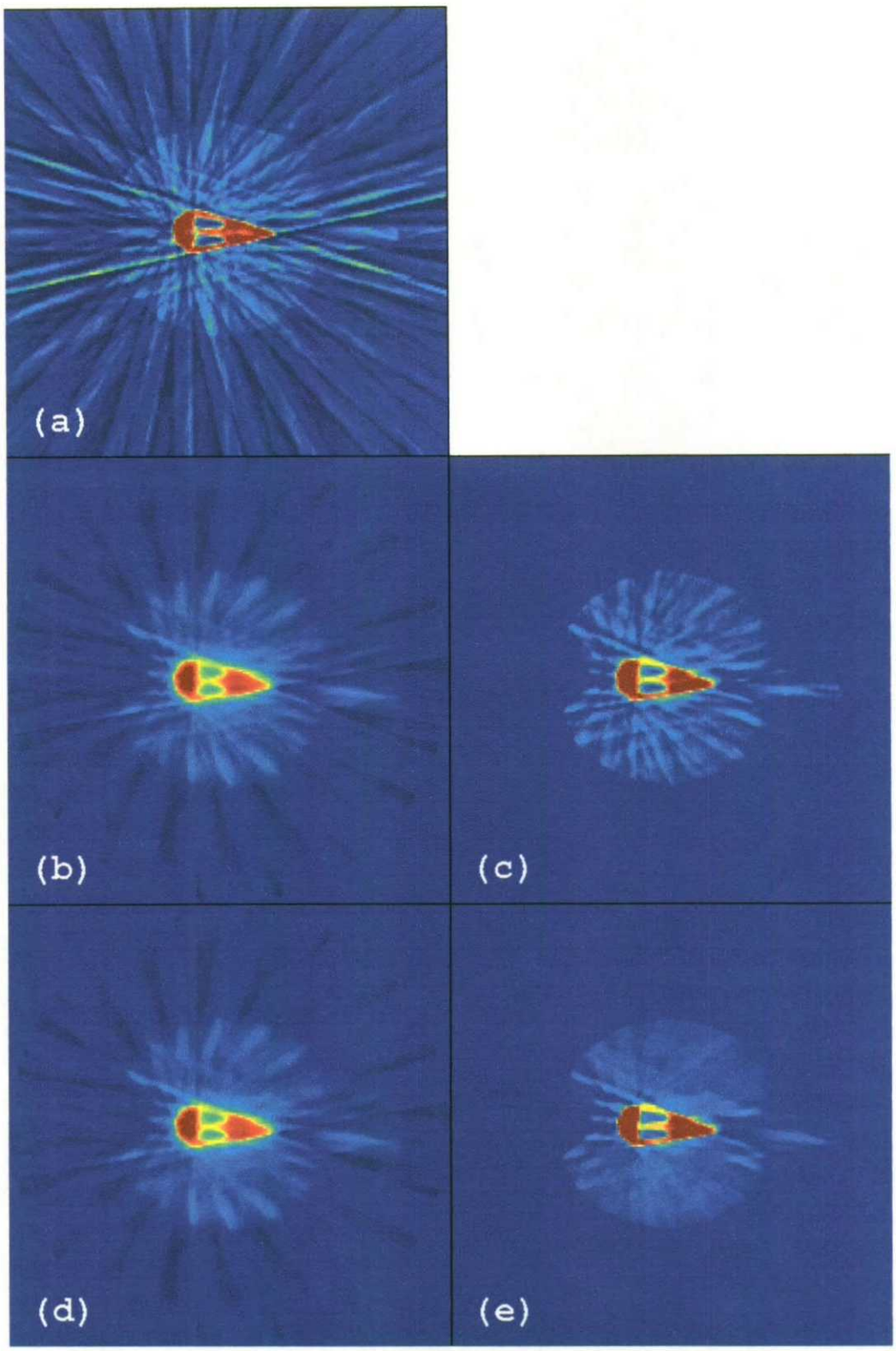

Figure 12. BCO4 slice-C 18-view reconstructions: (a) FBP; (b) SVD; (c) pSVD; (d) TV; and (e) TV-SVD.

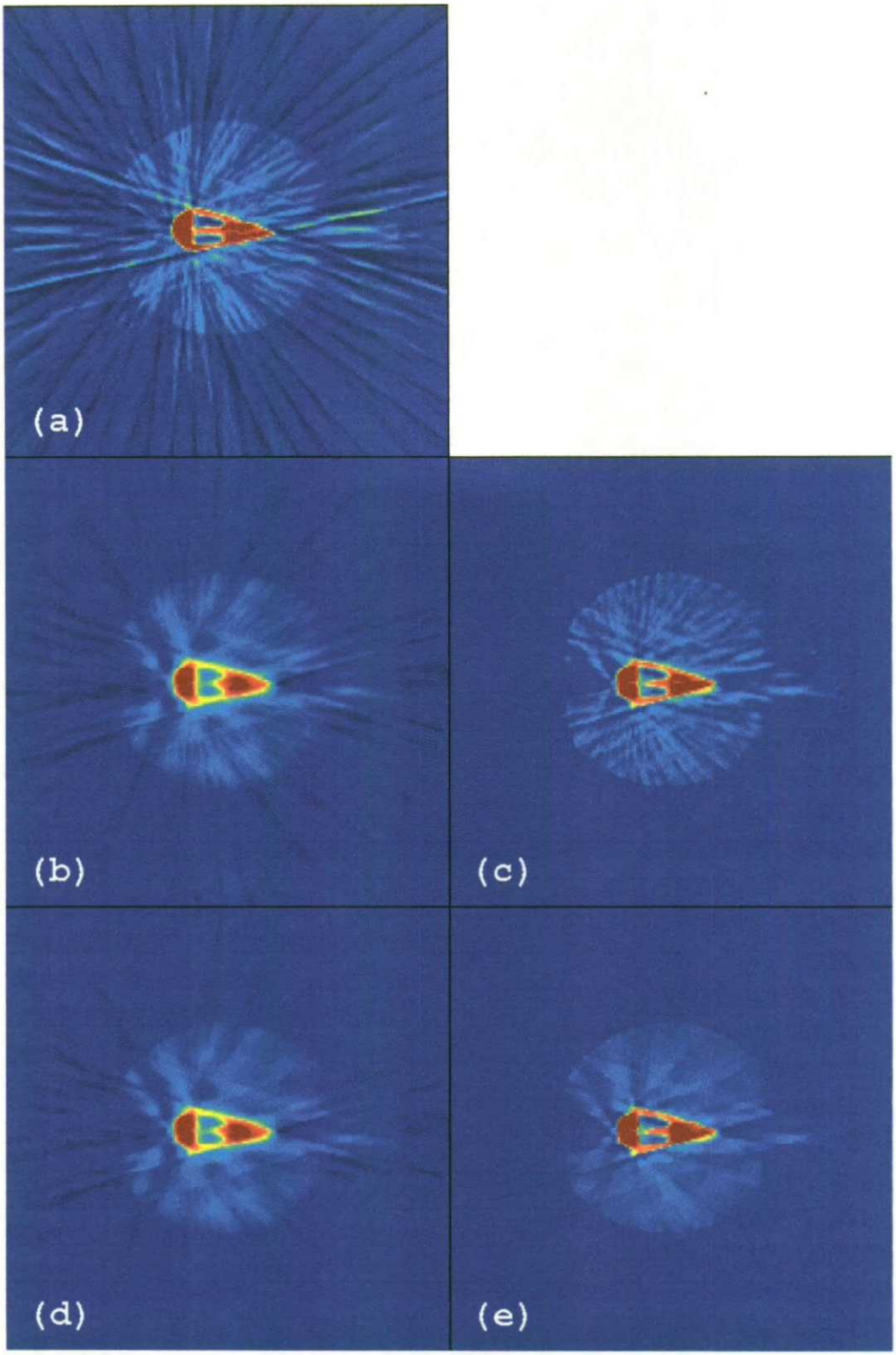

Figure 13. BCO4 slice-C 24-view reconstructions: (a) FBP; (b) SVD; (c) pSVD; (d) TV; and (e) TV-SVD.

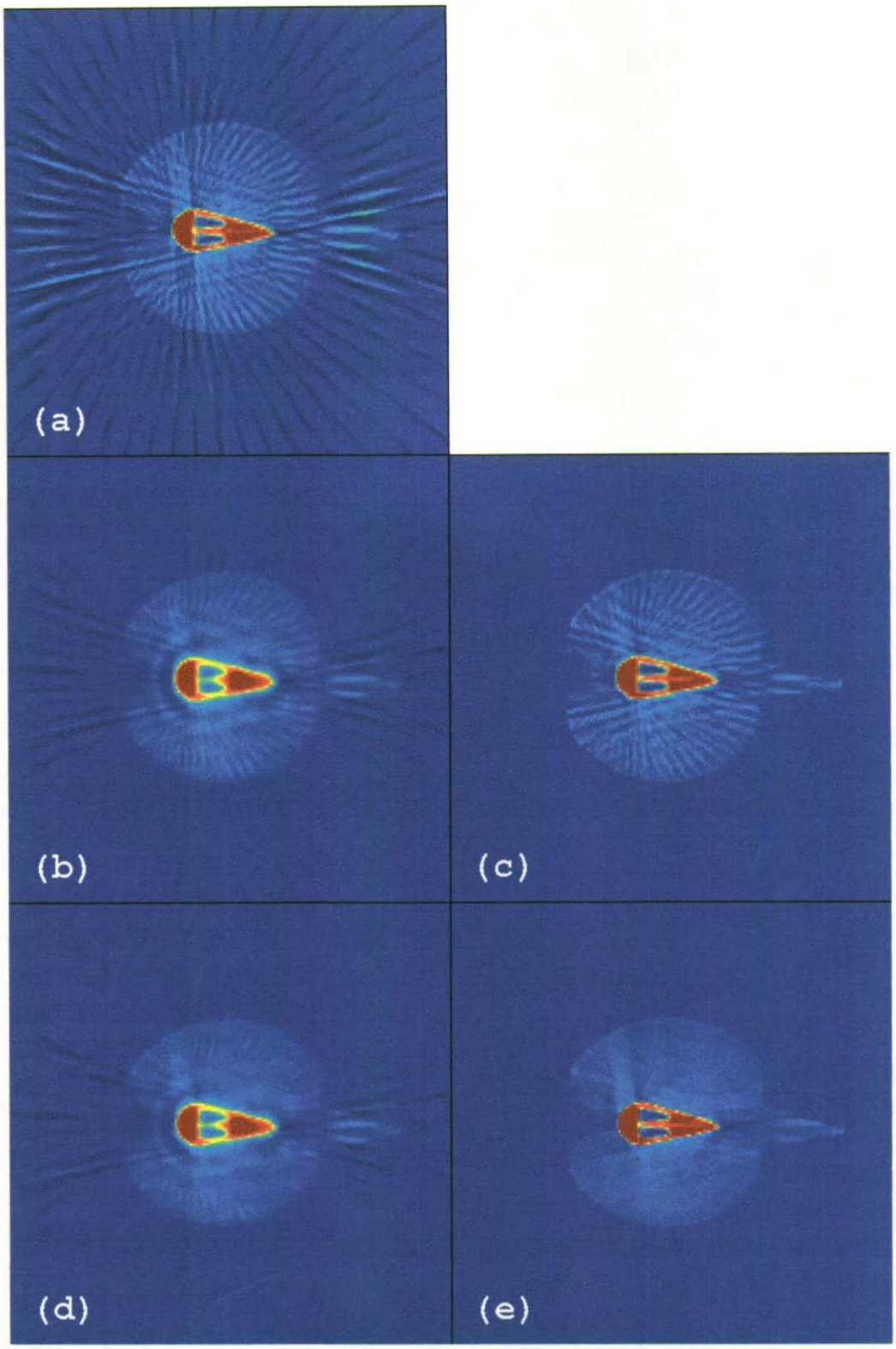

Figure 14. BCO4 slice-C 30-view reconstructions: (a) FBP; (b) SVD; (c) pSVD; (d) TV; and (e) TV-SVD.

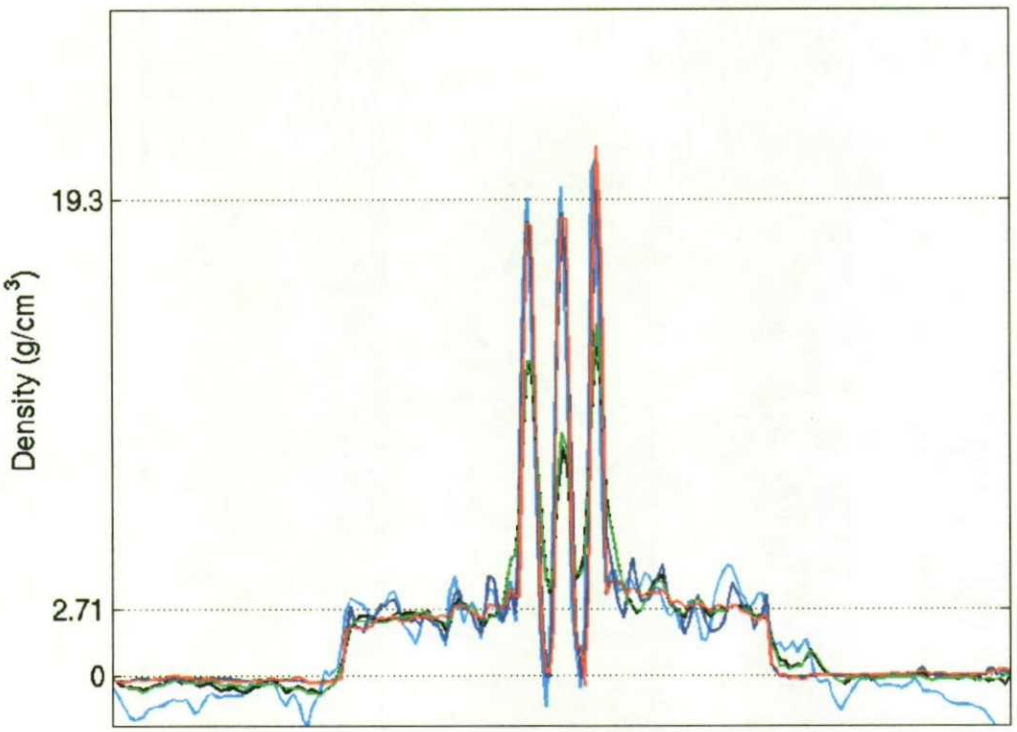

Figure 15. Density lineout *c* of the reconstructions in Fig. 14. The five colors represent the following reconstruction methods (cyan) FBP; (black) SVD; (blue) pSVD; (green) TV; and (red) TV-SVD.

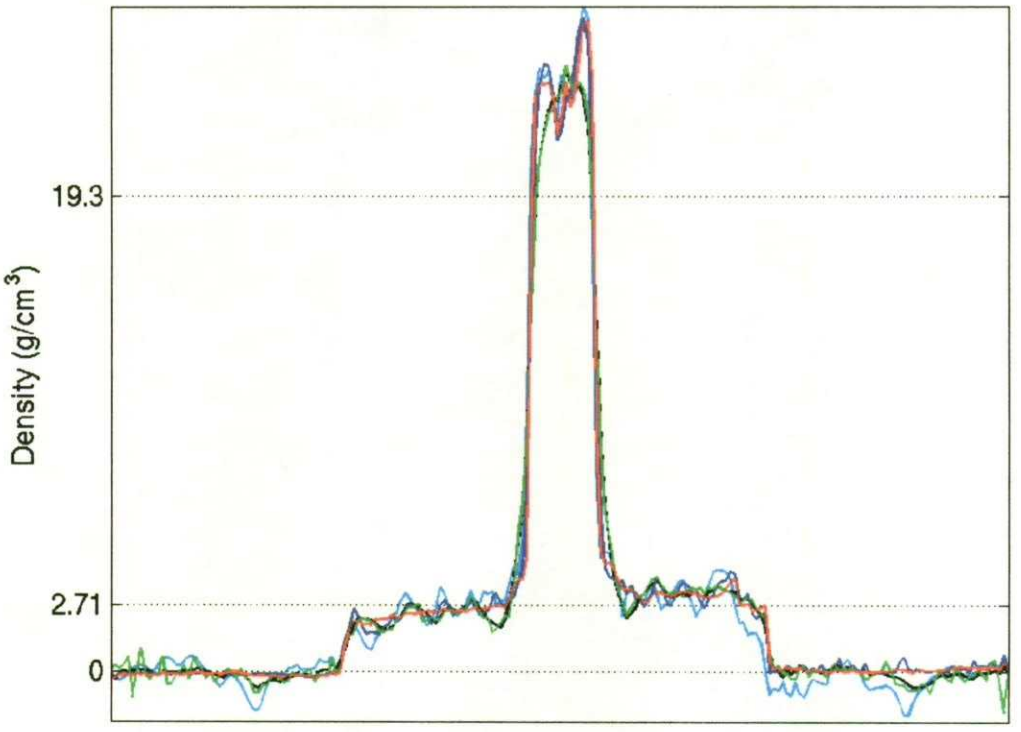

Figure 16. Density lineout *b* of the reconstructions in Fig. 10. The five colors represent the following reconstruction methods (cyan) FBP; (black) SVD; (blue) pSVD; (green) TV; and (red) TV-SVD.

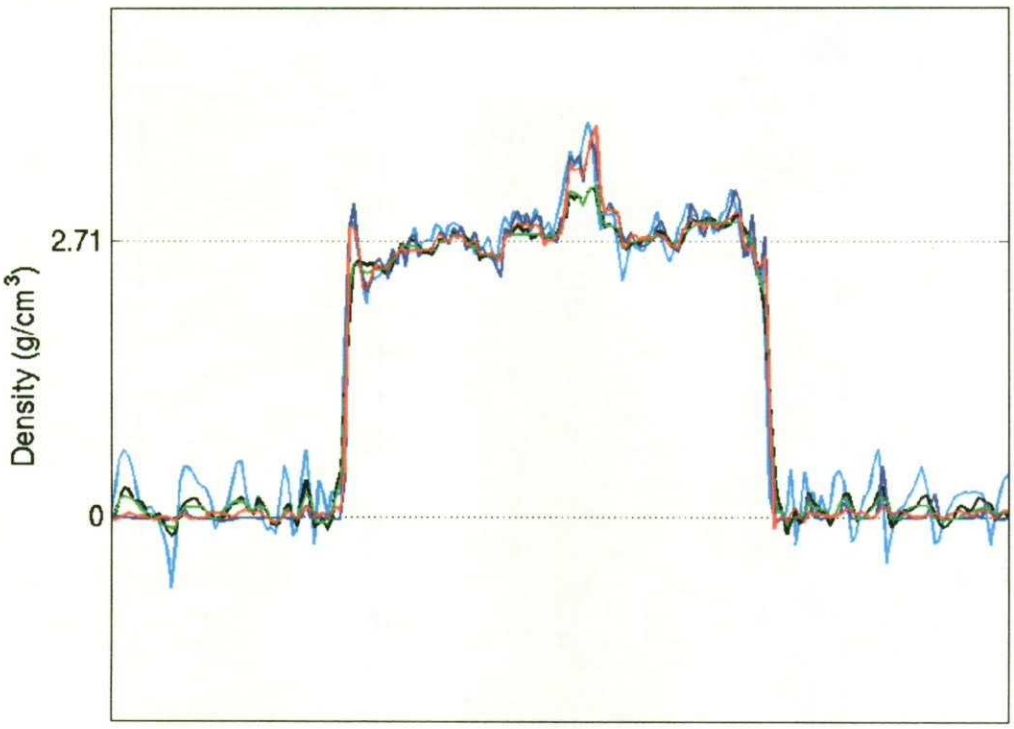

Figure 16. Density lineout *a* of the reconstructions in Fig 6. The five colors represent the following reconstruction methods (cyan) FBP; (black) SVD; (blue) pSVD; (green) TV; and (red) TV-SVD.